Original Article

Influences of the second motion probing gradient *b*-value and T2 relaxation time on magnetic resonance diffusion-derived 'vessel density' (DDVD) calculation: the examples of liver, spleen, and liver simple cyst

Zhi-Guo Ju[1#], Xiao-Ming Leng[2#], Ben-Heng Xiao[3#], Ming-Hua Sun[3,4], Hua Huang[5], Gen-Wen Hu[6], Ge Zhang[7], Ji-Hong Sun[8], Michael S. Y. Zhu[9], Giuseppe Guglielmi[10,11], Yì Xiáng J. Wáng[3]^

[1]College of Medical Imaging, Shanghai University of Medicine and Health Science, Shanghai, China; [2]Universal Medical Imaging Diagnostic Center of Guangzhou, Guangzhou, China; [3]Department of Imaging and Interventional Radiology, Faculty of Medicine, The Chinese University of Hong Kong, Shatin, New Territories, Hong Kong SAR, China; [4]Department of Radiology, Fuyang Hospital of Anhui Medical University, Fuyang, China; [5]Department of Radiology, The Third People's Hospital of Shenzhen, Shenzhen, China; [6]Department of Radiology, Shenzhen People's Hospital, The Second Clinical Medical College, Jinan University, Shenzhen, China; [7]Department of Radiology, Zhujiang Hospital, Southern Medical University, Guangzhou, China; [8]Department of Radiology, Sir Run Run Shaw Hospital, Zhejiang University School of Medicine, Hangzhou, China; [9]Yingran Medicals Co., Ltd., Hong Kong SAR, China; [10]Department of Clinical and Experimental Medicine, Foggia University School of Medicine, Foggia, Italy; [11]Radiology Unit, Dimiccoli Teaching Hospital Barletta, Barletta, Italy

Contributions: (I) Conception and design: YXJ Wáng; (II) Administrative support: ZG Ju, XM Leng, BH Xiao, MSY Zhu, G Guglielmi; (III) Provision of study materials or patients: H Huang, GW Hu, G Zhang; (IV) Collection and assembly of data: ZG Ju, XM Leng, H Huang, GW Hu, G Zhang; (V) Data analysis and interpretation: BH Xiao, MH Sun, JH Sun, YXJ Wáng; (VI) Manuscript writing: All authors; (VII) Final approval of manuscript: All authors.

[#]These authors contributed equally to this work.

Correspondence to: Yì Xiáng J. Wáng, PhD. Department of Imaging and Interventional Radiology, Faculty of Medicine, The Chinese University of Hong Kong, 30-32 Ngan Shing Street, Shatin, New Territories, Hong Kong SAR, China. Email: yixiang_wang@cuhk.edu.hk.

Background: Magnetic resonance (MR) diffusion-derived 'vessel density' (DDVD) is calculated according to: $DDVD_{b0b2}$ = Sb0/ROI_{area0} – S_{b2}/ROI_{area2}, where S_{b0} and S_{b2} refer to the tissue signal when *b*-value is 0 or 2 s/mm^2. S_{b2} and ROI_{area2} can also be approximated by other low *b*-values diffusion-weighted imaging (DWI). This study investigates the influence of the second motion probing gradient *b*-value and T2 on DDVD calculations of the liver, spleen, and liver simple cyst. Literature analysis shows the liver and spleen have very similar amounts of perfusion. At 3T, liver and spleen have a T2 of around 42 and 60 ms respectively, while cyst has a very long T2.

Methods: Twenty-eight subjects had 1.5T DWI data with *b*-values of 0, 1, 2, 15, 20, 30 s/mm^2. Twenty-one subjects had 3.0T DWI data with *b*-values of 0, 2, 4, 7, 10, 15, 20, 30 s/mm^2. $DDVD_{b0b1}$, $DDVD_{b0b2}$, $DDVD_{b0b4}$, $DDVD_{b0b7}$, $DDVD_{b0b10}$, $DDVD_{b0b15}$, $DDVD_{b0b20}$, and $DDVD_{b0b30}$ were calculated from *b*=0 and *b*=1 images, *b*=0 and *b*=2 images, *b*=0 and *b*=4 images, *b*=0 and *b*=7 images, *b*=0 and *b*=10 images, *b*=0 and *b*=15 images, *b*=0 and *b*=20 images, *b*=0 and *b*=30 s/mm^2 images, respectively. For liver simple cyst, two cysts totaling six slices scanned at 1.5T were available for DDVD measurement.

Results: At 1.5T, when the second *b*-value was 1 s/mm^2, $DDVD_{spleen}$ value was slightly higher than $DDVD_{liver}$ value; when the second *b*-value was 2 s/mm^2, $DDVD_{liver}$ value was slightly higher than $DDVD_{spleen}$ value. After that, the absolute difference between $DDVD_{liver}$ value and $DDVD_{spleen}$ value became increasingly larger,

^ ORCID: 0000-0001-5697-0717.

with $DDVD_{liver}$ value being consistently higher. $DDVD_{cyst}$ showed values close to 0 when the second *b*-value was 1 s/mm^2. When the second *b*-value was 20 or 30 s/mm^2, $DDVD_{cyst}$ value was higher than $DDVD_{liver}$ value. The absolute DDVD values measured higher at 3.0T than at 1.5T. However, the ratio of $DDVD_{spleen}$ to $DDVD_{liver}$ did not apparently differ between 1.5T and 3.0T. From the second *b*-value being 2 s/mm^2 onward, an increasingly larger second *b*-value was associated with a trend of slow decreasing of the ratio of $DDVD_{spleen}$ to $DDVD_{liver}$.

Conclusions: When a very low second *b*-value is applied, the liver and spleen measure similar perfusions by DDVD, and cysts measure DDVD close to zero. When a higher second *b*-value is applied, relative to the liver, the DDVD of spleen is suppressed while the DDVD of cyst is artificially promoted, which we consider are related to the T2 relaxation times of the liver, spleen, and cyst.

Keywords: Magnetic resonance imaging (MRI); perfusion; T2 relaxation time; diffusion-derived 'vessel density' (DDVD)

Submitted Nov 02, 2024. Accepted for publication Dec 10, 2024. Published online Dec 18, 2024.
doi: 10.21037/qims-24-2411
View this article at: https://dx.doi.org/10.21037/qims-24-2411

Introduction

Our exploration of diffusion-weighted imaging (DWI) in liver fibrosis evaluation revealed that diffusion-derived 'vessel density' (DDVD) could potentially reflect microvascular perfusion. For spin-echo type echo-planar sequence, the second motion probing gradient after the 180-degree radiofrequencey pulse cannot fully re-focus the flowing spins in vessel and micro-vessels after being de-phased by the first motion probing gradient before the 180-degree RF pulse. Therefore, liver blood vessels including sub-pixel microvessels show high signal when there is no motion probing gradient (*b*=0 s/mm^2) and low signal when even very low *b*-values (such as *b*=1, *b*=2 s/mm^2) are applied (*Figure 1*) (1). Thus, the signal difference between images when the motion probing gradient is 'off' and 'on' reflects the extent of tissue vessel density in physiological sense, and we term this as DDVD. DDVD [unit: arbitrary unit (au)/pixel] is derived from the Eq. [1]:

$$DDVD_{b0b2} = S_{b0} / ROI_{area0} - S_{b2} / ROI_{area2} \quad [1]$$

where ROI_{area0} and ROI_{area2} refer to the number of pixels in the selected region-of-interest (ROI) on *b*=0 and *b*=2 s/mm^2 DWI, respectively. S_{b0} refers to the measured sum signal intensity within the ROI when *b*=0, and S_{b2} refers to the measured sum signal intensity within the ROI when *b*=2 s/mm^2, thus S_b/ROI_{area} equates to the mean signal intensity within the ROI. S_{b2} and ROI_{area2} can also be approximated by other low *b*-values (such as *b*=10 s/mm^2) DWI. In our initial testing (1), with 20 healthy livers, 11 stage-1 fibrotic livers, and 5 stage-4 fibrotic livers, mean DDVD was 26.5 for healthy livers, 21.8 for stage-1 fibrotic livers, and 12.1 for stage-4 fibrotic livers (1) (approach shown on *Figure 1*). If we consider a pixel to be an individual ROI, DDVD pixelwise map can be constructed pixel-by-pixel with this same principle (2).

The analysis of DDVD requires only two *b*-values (with one being *b*=0 s/mm^2 and the other being non-zero low *b*-value), with a significantly shorter scanning time than contrast enhanced computed tomography (CT)/magnetic resonance imaging (MRI) while without the need of a contrast agent injection. DDVD is conceptually as simple as the apparent diffusion coefficient (ADC). DDVD measure based on this simple principle appears to be useful as a straightforward imaging biomarker in diverse clinical scenarios. Huang *et al.* (3) showed that DDVD analysis demonstrates liver parenchyma has an age-dependent decrease of micro-perfusion in healthy women. This agrees with the known physiological age-dependent reduction in liver blood flow which has been well documented using a variety of technical methods including histology, dye dilution, indicator clearance. DDVD is a useful parameter for distinguishing livers with and without fibrosis, and livers with more severe fibrosis tend to have even lower DDVD measurements than those with milder liver fibrosis (1,4,5). With DDVD analysis, Zheng *et al.* (6) demonstrated that per unit micro-circulation of spleen is decreased in viral hepatitis-B liver fibrosis patients, and this reduction in micro-circulation is associated with the severity of liver

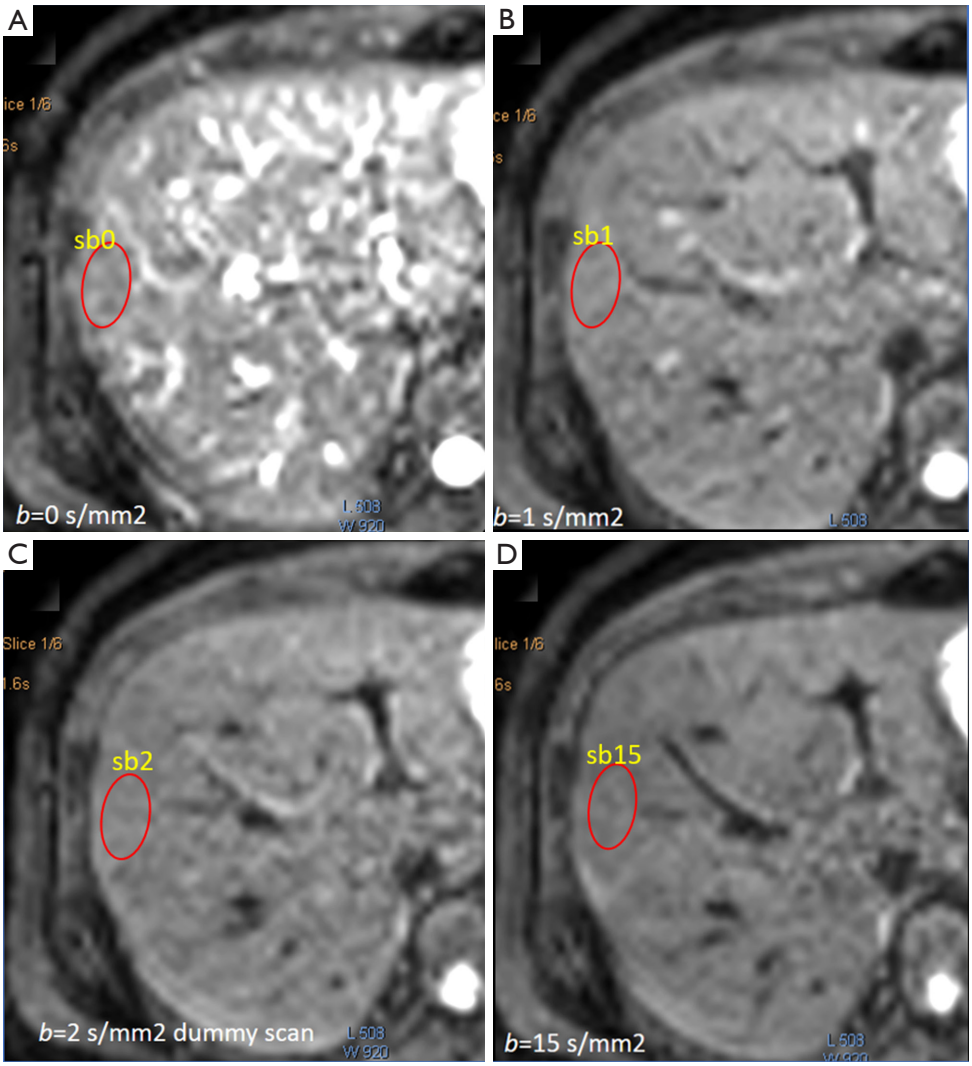

Figure 1 1.5 T liver diffusion weighted images with *b*-value of 0 (A), 1 (B), 2 (C), 15 s/mm^2 (D). Dummy scan (C) was scanned ahead of *b*=0 image (A). The signal difference between *b*=0 s/mm^2 image and *b*=1 or 2 s/mm^2 images is dramatic, particularly the vessels show high signal when the motion probing gradient is 'off' while showing dark signal when the motion probing gradient is 'on' even at *b*=1 s/mm^2. The high intensity of the vasculature seen on *b*=0 s/mm^2 image led to the naming of diffusion derived 'vessel density'.

fibrosis. This is consistent with earlier radioisotope imaging or CT perfusion studies where splenic blood flow (unit in mL/min/mL) was decreased in liver fibrosis patients (7-10), though total splenic blood flow, calculated multiplying specific splenic flow by spleen volume, was increased. He *et al*. (11) and Li *et al.* (12) reported that placenta DDVD as a perfusion biomarker allows excellent separation of normal and early pre-eclampsia pregnancies. Lu *et al*. (13) reported that placenta regional DDVD is significantly higher in pregnant women with placenta accreta spectrum disorders than women with normal placenta, and especially higher in patients with placenta percreta. Hu *et al.* (14) described that liver hemangiomas can be mostly differentiated from liver mass-forming lesions [hepatocellular carcinomas (HCCs) and focal nodular hyperplasia] solely based on DDVD map. Chen *et al.* (15) described a proof-of-concept study that a combination of DDVD map and high *b*-value DWI identifies the exitance and the size of penumbras.

As absolute magnetic resonance (MR) signal intensity is influenced by various factors, including B0/B1 spatial inhomogeneity, coil loading, receiver gain, etc., we use the ratio of a lesion to its adjacent native tissue (such as

the ratio of HCC's DDVD to liver DDVD) to minimize these scaling factors. Li *et al.* (16) applied DDVD to assess the perfusion of HCC. DDVD results (ratio of HCC DDVD to background liver DDVD) approximately agree with other dynamic contrast enhanced CT/MRI literature data (17-19). Lu *et al.* (20) reported earlier clinical grades rectal carcinoma had a higher DDVD ratio (tumor to tumor-free rectal wall) than those of the advanced clinical grades. This is consistent with the biological behaviors of rectal carcinoma (21). In one study, we used DDVD ratio (DDVDr) to evaluate 24 pleomorphic adenomas (PAs), 14 malignant tumors, and 16 Warthin's tumors. DDVDr was DDVD of the tumor divided by DDVD of tumor free parotid gland tissue. A systematic literature search was conducted for parotid gland tumor perfusion imaging and histology microvessel density studies. Perfusion parameters of PAs, malignant tumors, and Warthin's tumors were further normalized by PA' measure (thus the normalized measure for PA is 1). The ratio results of malignant tumor DDVD and Warthin's tumors DDVDr were compared with literature results. In the cases of parotid gland tumors, DDVD appears to offer more consistent and comparable results (comparable to CT and histology microvessel density results) than arial spin labeling and intravoxel incoherent motion (IVIM) [briefly summarized in (15)].

In clinical practice, it is highly likely that DDVD protocol users in different MRI scanner settings will select different second non-zero low *b*-value. Most of the Philips scanners allow the selection of b=1, b=2 s/mm^2, etc., while some other scanners only allow the lowest non-zero *b*-value to be 10, or 20 s/mm^2. To facilitate the comparison of at least relative DDVD values (relative DDVD means absolute DDVD of one tissue is normalized by absolute DDVD of another reference tissue) cross different MRI scanners, taking the cases of liver, spleen, liver simple cyst as examples, this study measures DDVD with the second non-zero low *b*-values ranging from 1 to 30 s/mm^2. Healthy liver and spleen are two large solid organs in the upper abdomen with similar amounts of blood perfusion as shown in *Table 1* (3,9,10,21-34) and *Table 2* (3,19,34-39) (liver perfusion being the sum of hepatic arterial perfusion and portal veinous perfusion), though it is likely that the liver has slightly higher blood volume (unit in mL/100 mL) due to the blood supply of portal vein and spleen has slightly higher blood flow (unit in mL/min/mL) due to the pure blood supply of the splenic artery. Compared with the liver, the spleen has longer T2 with higher contact of free water (23-25,40), thus DDVD data of the liver and the spleen allow us to study how DDVD measure is affected by T2. One of the perceived advantages of DDVD over ADC and IVIM imaging is that, when we use DWI images of b=0 and a non-zero very low *b*-value to calculate DDVD, DDVD is minimally affected by T2. On the other hand, both diffusion metrics of IVIM and ADC are heavily contributed by T2 (34,41-44). Conventional IVIM-perfusion fraction (PF) is known to be affected by tissue's T2 time, with longer T2 time leading to a 'depressed' PF measure (16,43). For example, Li *et al.* (16) showed most HCCs have higher DDVD (calculated from b=0 and b=2 mm^2/s DWI or calculated from b=0 and b=10 mm^2/s DWI) which is consistent with histology and CT/MRI results. However, most IVIM reports described a lower PF for HCC than for adjacent liver parenchyma (16,43). DDVD results (calculated from b=0 and b=2 mm^2/s DWI) show the liver and spleen have very similar perfusion (6), while most IVIM reports described spleen PF is only half of that of the liver (45). While ADC is a composite biomarker influenced by many factors, ADC measure is more affected by T2 than by diffusion (42,43,46). For example (46), abscess liquid (pus) has a very low ADC of around 0.65×10^{-3} mm^2/s due to its T2 being 80 ms; articular cartilage has a high ADC of around 1.5×10^{-3} mm^2/s due to its short T2 (around 40 ms at 3.0T), chondrosarcoma has a high ADC of around 2.3×10^{-3} mm^2 due to its long T2 time (around e.g., 120 ms). These values are not reasonable for a metric expected to reflect *in vivo* diffusion (46).

Methods

This is a restrospective analysis of previously prospectively acquired liver IVIM data. All IVIM data were acquired with institutional ethical approval and with informed consent obtained from individual participants (14,47). Data acquisition protocols are listed in the Appendix 1. 1.5T IVIM DWI data included 26 healthy volunteers (14 males, 12 females, mean age: 24 years old; range, 20–41 years old) and two liver fibrosis patients (2 males, aged 45 years and 49 years respectively). 3.0T IVIM DWI data included 19 healthy volunteers (10 males, 9 females, mean age: 33 years old; range, 22–65 years old) and 2 liver fibrosis patients (1 male aged 60 years and 1 female, aged 47 years).

All image processing was implemented in a custom program developed on MATLAB (Mathworks, Natick, MA, USA). DWI data with *b*-values of 0, 1, 2, 15, 20, 30 s/mm^2 were used for 1.5T MRI, and DWI data with *b*-values of 0, 2, 4, 7, 10, 15, 20, 30 s/mm^2 were used for 3.0T MRI. On

Table 1 Liver and spleen iron concentration, MRI relaxation times, and blood flow

Study	Subjects	Parameter	Liver[¶]	Spleen[¶]
Sorokin *et al.* (22)	Community population	Iron concentration, mg/g	1.24±0.29	0.92±0.32
Schwenzer *et al.* (23)	Normal subjects	T2* (ms) 1.5 T	28.1±7.1	43.9±20.6
de Bazelaire *et al.* (24)	Normal subjects	T2 (ms) 1.5 T	46±6	79±15
		T2 (ms) 3.0 T	34±4[#]	61±9
		T1 (ms) 1.5 T	586±39	1,057±42
		T1 (ms) 3.0 T	809±71	1,328±31
Bogaert *et al.* (25)	Normal controls	T2 (ms) 1.5 T	46±4	
		T1 (ms) 1.5 T	540±34	
Tsushima *et al.* (26)	Normal controls	CTP	1.132	1.35±0.44
Taniguchi *et al.* (27)	Patients of no liver disease	NMP	1.257	1.333
Tsushima *et al.* (9)	Patients of no spleen disease, some with liver metastasis	CTP		1.30±0.43
Miles *et al.* (10)	Patients of no spleen disease, some with liver metastasis	CTP		1.4±0.3
Blomley *et al.* (28)	No spleen disease patients	CTP		1.29±0.11
Blomley *et al.* (29)	Controls	CTP	1.11±0.07	
Bader *et al.* (30)	Normal controls	CTP	1.22±0.39	
Bader *et al.* (31)	Normal controls	CTP	1.38±0.32	
Oguro *et al.* (32)	Patients of no liver disease	NMP		1.603
Yasuhara *et al.* (33)	Patients of no liver disease	NMP	1.308	

For blood flow, different authors reported slightly different values (which may be affected by the data acquisition and data processing protocols) and this may be also due to that liver/spleen blood flows vary with gender and age (3,34). [¶], mixed male and female population, with values in mean or mean ± standard deviation. The results of Blomley *et al.* are in mean ± standard error of the mean. [#], value probably estimated too short. CTP, blood flow (unit: mL/min/mL) measured with computed tomography perfusion method; NMP, blood flow (unit: mL/min/mL) measured with nuclear medicine perfusion method; MRI, magnetic resonance imaging.

each DW image for the liver and spleen, ROIs were drawn to cover a large portion of the right liver parenchyma and spleen parenchyma while avoiding large vessels and artifacts. Based on Eq. [1], $DDVD_{b0b1}$, $DDVD_{b0b2}$, $DDVD_{b0b4}$, $DDVD_{b0b7}$, $DDVDb_{0b10}$, $DDVD_{b0b15}$, $DDVD_{b0b20}$, and $DDVD_{b0b30}$ were calculated from b=0 and b=1 images, b=0 and b=2 images, b=0 and b=4 images, b=0 and b=7 images, b=0 and b=10 images, b=0 and b=15 images, b=0 and b=20 images, b=0 and b=30 s/mm^2 images, respectively. For each study subject, the mean signal intensity of each ROI was weighted by the number of pixels included in each ROI relative to total ROI area in a subject, then the sum of the weighted DDVDs was calculated to obtain the value for each liver and spleen. For liver simple cysts (from the two liver fibrosis patients scanned at 1.5T), only two cysts (size =26.8 and 36.3 mm) totaling six slices were available for DDVD measurement.

Influences of the second b-value on DDVD were compared for liver, spleen, and liver simple cyst, and compared between 1.5T results and 3.0T results. Data are presented graphically.

Results

For 1.5T data, the plotted data between the second b-values for DDVD calculation and liver, spleen, or cyst DDVD values are shown in *Figures 2*,*3*. It is noted that, when the second b-value was 1 s/mm^2, $DDVD_{spleen}$ value was slightly higher than $DDVD_{liver}$ value; when the second b-value was 2 s/mm^2, $DDVD_{liver}$ value was slightly higher than

Table 2 A comparison of CT measured blood volumes of the liver and the spleen in various type of patients

Study	Subjects	Liver[¶]	Spleen[¶]
Zhu *et al.* (35)	Cirrhosis patients, no severe portal hypertension	17.4±3.6	14.9±2.9
Wang *et al.* (36)	Moderate portal hypertension patients	19.7±3.0	13.9±2.9
Wang *et al.* (36)	Severe portal hypertension patients	15.5±2.2	11.9±2.5
Gadupudi *et al.* (37)	Liver of hemangioma patients	13.6	
Gadupudi *et al.* (37)	Liver of HCC patients	15.12	
Ippolito *et al.* (19)	Cirrhosis and HCC patients	10.9	
Yan *et al.* (38)	Non-high-risk esophageal varices patients		14.99±6.06
Yan *et al.* (38)	High-risk esophageal varices patients		16.17±5.69
Sauter *et al.* (39)	No liver and spleen disease patients		16.39±4.64
Sauter *et al.* (39)	Cirrhosis and HCC patients		13.91±6.46

Different authors reported slightly different values (which may be affected by the data acquisition and data processing protocols) and this may be also due to that liver/spleen blood flows vary with gender and age (3,34). [¶], mixed male and female population, with values (unit: mL/100 mL) in mean or mean ± standard deviation. HCC, hepatocellular carcinoma; CT, computed tomography.

$DDVD_{spleen}$ value. After that, the absolute difference between $DDVD_{liver}$ value and $DDVD_{spleen}$ value became increasingly larger, with $DDVD_{liver}$ value being consistently higher. $DDVD_{cyst}$ showed a value close to 0 when the second *b*-value was 1 s/mm^2, and a low value when the second *b*-value was 2 s/mm^2. When the second *b*-value was 20 or 30 s/mm^2, $DDVD_{cyst}$ values were higher than the $DDVD_{liver}$ value.

The relationship between the second *b*-values and the $DDVD_{liver}$ values at 1.5T was fitted by

$$1.5T\ DDVD_{liver} = 5.654 * \ln\left(2^{nd} b\right) + 8.915 \quad [2]$$

The relationship between the second *b*-values and spleen $DDVD_{spleen}$ values at 1.5T was fitted by

$$1.5T\ DDVD_{spleen} = 4.270 * \ln\left(2^{nd} b\right) + 9.225 \quad [3]$$

The relationship between the second *b*-values and liver cyst DDVD values at 1.5T was linearly fitted by (48):

$$1.5T\ DDVD_{cyst} = DDVD = 2.009 * \left(2^{nd} b\right) - 2.982 \quad [4]$$

DDVD pixelwise maps of two cases of liver simple cysts at 1.5T are shown in *Figure 4*.

For 3.0T data, the plotted data between the second *b*-values for DDVD calculation and liver or spleen DDVD values are shown in *Figure 5*. When the second *b*-value was 2 s/mm^2, $DDVD_{liver}$ was already higher than $DDVD_{spleen}$. After that, the absolute difference between $DDVD_{liver}$ value and spleen $DDVD_{spleen}$ value became increasingly larger.

The relationship between the second *b*-values and the $DDVD_{liver}$ values at 3.0T was fitted by

$$3.0T\ DDVD_{liver} = 10.082 * \ln\left(2^{nd} b\right) + 28.859 \quad [5]$$

The relationship between the second *b*-values and spleen $DDVD_{spleen}$ values at 3.0T was fitted by

$$3.0T\ DDVD_{spleen} = 5.863 * \ln\left(2^{nd} b\right) + 30.494 \quad [6]$$

Measured DDVD values are also shown in *Table 3*, and the ratios of $DDVD_{spleen}$ to $DDVD_{liver}$ are shown in *Figure 6*. A comparison of 1.5T data and 3.0T data shows the absolute DDVD values measured higher at 3.0T than at 1.5T, and the absolute DDVD difference between the liver and spleen was greater at 3.0T than at 1.5T, even when the second *b*-value was 2 s/mm^2. However, the ratios of $DDVD_{spleen}$ to $DDVD_{liver}$ did not apparently differ between 1.5T and 3.0T. From the second *b*-value being 2 s/mm^2 onward, an increasingly larger second *b*-value was associated with a trend of slow decreasing of the ratio of $DDVD_{spleen}$ to $DDVD_{liver}$. For 3T data, $DDVD_{spleen}$ to $DDVD_{liver}$ ratio was 0.790 when the second *b*-value was 30 s/mm^2.

Discussion

In our earlier studies, we used various second *b*-values for

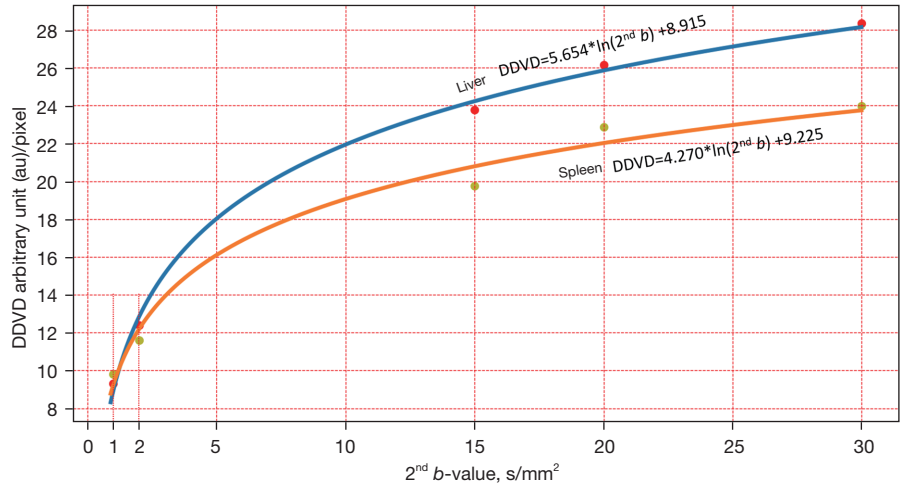

Figure 2 Fitted data of 1.5T liver and spleen DDVD median values over second *b*-values, data of 28 subjects (16 males, 12 females) among them two male cases were with liver fibrosis. DDVD, diffusion derived 'vessel density'.

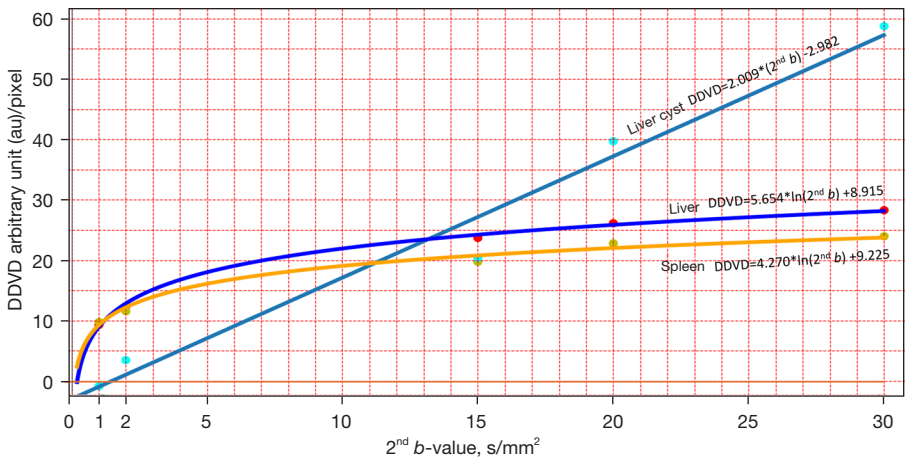

Figure 3 Fitted data of 1.5T liver, spleen, and liver cyst DDVD median values over second *b*-values. Liver and spleen data are from 28 subjects. Liver cyst data are based on two cysts totaling six slices from two male patients with liver fibrosis. DDVD, diffusion derived 'vessel density'.

DDVD calculation. In some studies, we used historical IVIM imaging data, thus the available lowest second *b*-value was utilized for DDVD calculation. In some prospective studies, the second *b*-value was constrained by the MRI scanners, as many MRI scanners do not allow the second *b*-value to be less than 10 s/mm^2. Since the perfusion status and T2 relaxation times of liver, spleen, and liver simple cysts are very well characterized, using the examples of liver, spleen, and liver cyst, this study aims to understand the impact of the second *b*-value for DDVD calculation, which we assume it is mainly moderated by T2. *Figure 2* shows, when the second b-value was 1, or 2 s/mm^2, the impact of T2 on DDVD was minimal, though that longer T2 (of the spleen relative to the liver) is associated with smaller DDVD could be noted even at very low second *b*-values (such as *b*=2 s/mm^2). From the second *b*-value being 2 s/mm^2 onward, an increasingly larger second *b*-value was associated with a slowly increasing contribution from T2, reflected by the slow decreasing trend of the ratio of $DDVD_{spleen}$ to $DDVD_{liver}$. It is interesting to note that, the ratio of spleen ADC to liver ADC appears to be in line with the ratio of $DDVD_{spleen}$ to $DDVD_{liver}$. *Figures 5,6* suggest the

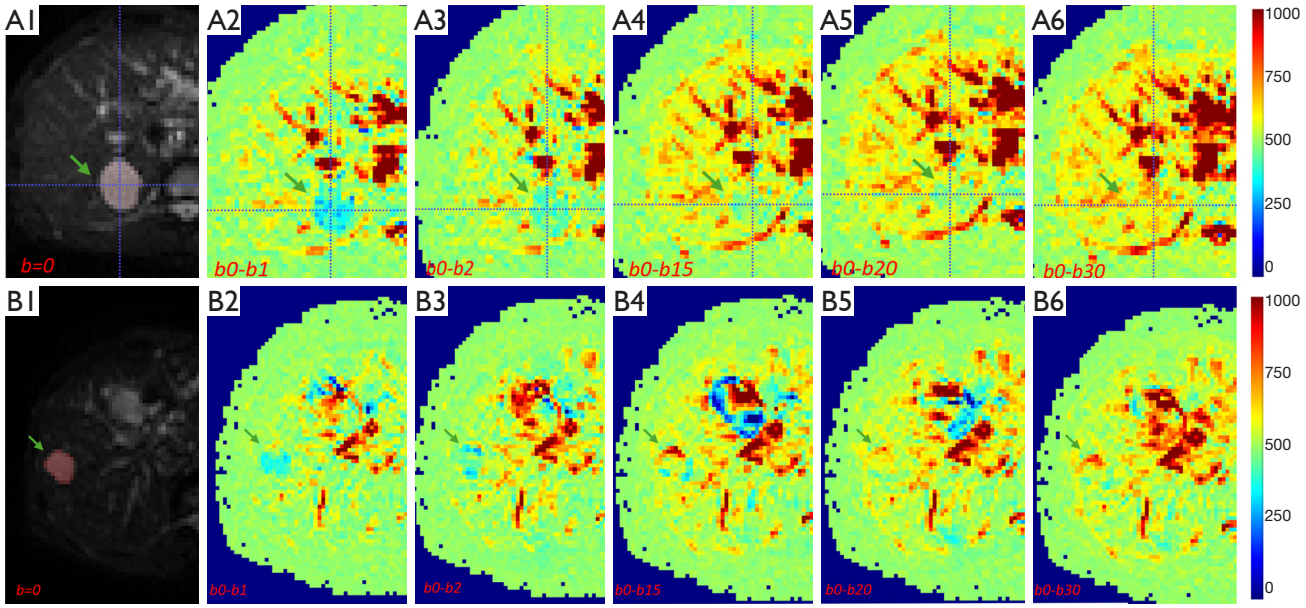

Figure 4 DDVD appearance of liver cysts (arrow) at 1.5T. *b*=0 diffusion-weighted imaging (A1,B1) and DDVD pixelwise maps with the second *b*-value being 1 (A2,B2), 2 (A3,B3), 15 (A4,B4), 20 (A5,B5), and 30 s/mm^2 (A6,B6), respectively. Due to the T2 contribution to DDVD values and together with possible misalignment between *b*=0 image and the second *b*-value image, typical DDVD appears is lost when second *b*-value is >15 s/mm^2. The cysts were marked with region-of-interest of red color on *b*=0 diffusion weighted image. DDVD, diffusion derived 'vessel density'.

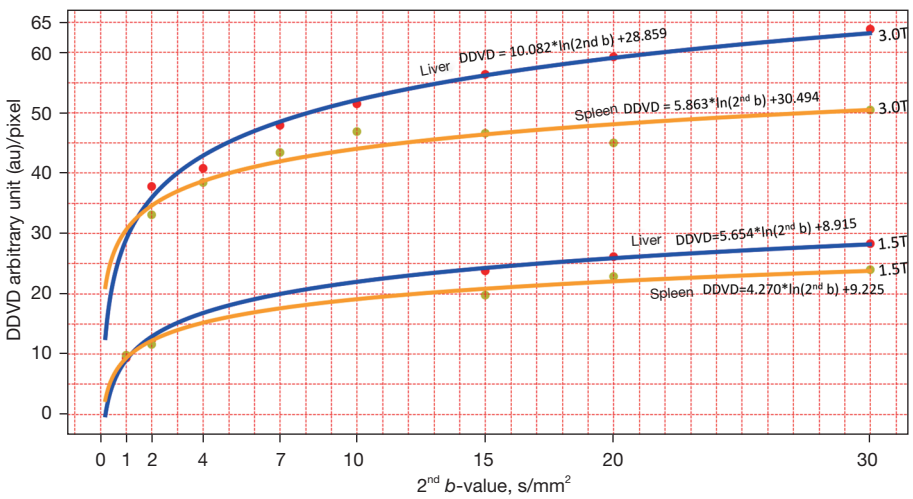

Figure 5 Fitted data of liver and spleen DDVD median values over second *b*-value, 1.5T and 3.0T data. 1.5T data are of 28 subjects (16 males, 12 females), among them two male cases were with liver fibrosis. 3.0T data are of 21 subjects (11 males, 10 females), among them one male case and one female case were with liver fibrosis. DDVD, diffusion derived 'vessel density'.

'fast diffusion' (i.e., perfusion) difference between liver and spleen may be modulated by T2. The ratio of spleen ADC to liver ADC appears to be in line with the ratio of $DDVD_{spleen}$ to liver $DDVD_{liver}$ suggests the possibility that the difference between the spleen ADC and liver ADC is also modulated by T2 (41,42). In other words, if the difference between spleen ADC and liver ADC is modulated by other factor(s), then the ratio of spleen ADC

Table 3 The second *b*-values and DDVD measures of liver parenchyma, spleen parenchyma, and liver cyst

2nd *b*-value (s/mm²)	1.5T DDVD values (au/pixel)			3T DDVD values (au/pixel)	
	Liver	Spleen	Liver cyst	Liver	Spleen
1	9.320 (7.49, 10.47)	9.815 (8.039, 12.665)	−0.793 (−43.50, 30.94)		
2	12.399 (10.53, 14.86)	11.587 (10.09, 13.67)	3.542 (−22.25, 40.37)	37.796 (27.50, 44.90)	33.125 (25.90, 43.64)
4				40.765 (31.37, 50.54)	38.433 (21.23, 51.05)
7				47.968 (36.06, 67.29)	43.395 (36.63, 59.99)
10				51.505 (38.29, 69.58)	46.857 (34.78, 57.23)
15	23.774 (21.12, 25.94)	19.738 (16.29, 22.95)	20.442 (−12.44, 46.04)	56.387 (43.99, 66.25)	46.617 (26.40, 55.65)
20	26.139 (23.16, 28.61)	22.854 (16.39, 28.60)	39.748 (18.36, 59.51)	59.316 (47.77, 69.80)	45.036 (35.80, 58.72)
30	28.346 (25.29, 31.54)	23.968 (19.70, 27.77)	58.794 (33.62, 89.16)	63.869 (51.53, 79.89)	50.480 (39.31, 61.47)

Data are presented as median (95% confidence interval). DDVD, diffusion-derived 'vessel density'; au, arbitrary unit.

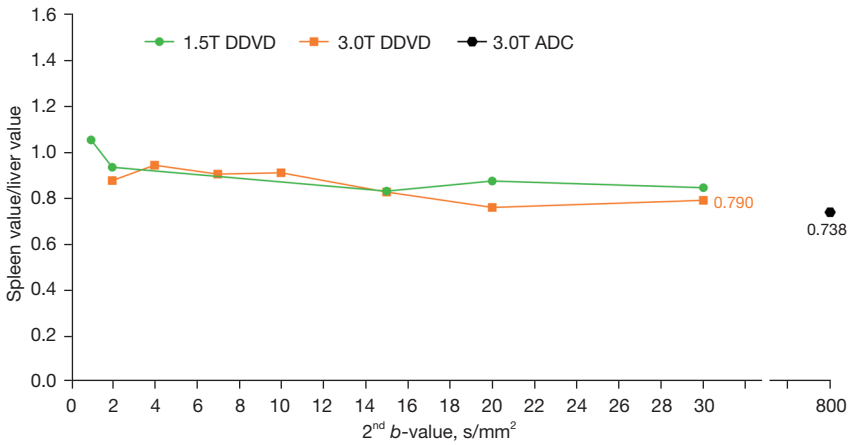

Figure 6 Ratios of $DDVD_{spleen}$ to $DDVD_{liver}$ over increasing second *b*-values, and ratio of spleen ADC to liver ADC from a literature report by Kim *et al.* (49). From second *b*-value being 2 s/mm² onward, an increasingly larger second *b*-value is associated with a slow decreasing trend of the ratio of $DDVD_{spleen}$ to $DDVD_{liver}$. Typical ADC data are from Kim *et al.* (spleen ADC 0.79, liver ADC 1.07×10^{-3} mm²/s, measured at 3.0 T with *b*-value of 0, 800 s/mm²). The ratio of spleen ADC to liver ADC appears to be in line with the ratio of $DDVD_{spleen}$ to $DDVD_{liver}$. DDVD, diffusion derived 'vessel density'; ADC, apparent diffusion coefficient.

to liver ADC would more likely differ from the ratio of $DDVD_{spleen}$ to $DDVD_{liver}$.

For diffusion MRI quantification of the liver and spleen, due to the longer spleen T2 (60 ms at 3T) than liver T2 (42 ms at 3T), both ADC and IVIM-PF are underestimated for the spleen values relative to the liver values (42,43). This may also cause a relative error for HCC ADC (42). HCC ADC has been traditionally noted to be with restricted diffusion. However, as HCCs are mostly associated with increased arterial blood supply and higher water content (i.e., edema, as shown with higher signal on T2-weighted image), we consider it unlikely that HCC has true lower diffusion, instead the lower HCC ADC is due to the longer T2 of HCC (HCC T2 is estimated to be close to that of spleen being around 60 ms) (42,50-52). On the other hand, measured by $DDVD_{b0b1}$ and $DDVD_{b0b2}$, the liver and spleen have very similar fast diffusion values. $DDVD_{b0b2}$ and $DDVD_{b0b10}$ also show higher values for HCC than for liver parenchyma (16). Thus, by minimizing the second *b*-value, the T2 effect on diffusion metrics can be largely mitigated with DDVD, and this may be an important advantage of DDVD over ADC and IVIM.

This study further demonstrated the practicality of DDVD in diagnosing liver simple cysts. Liver cysts typically

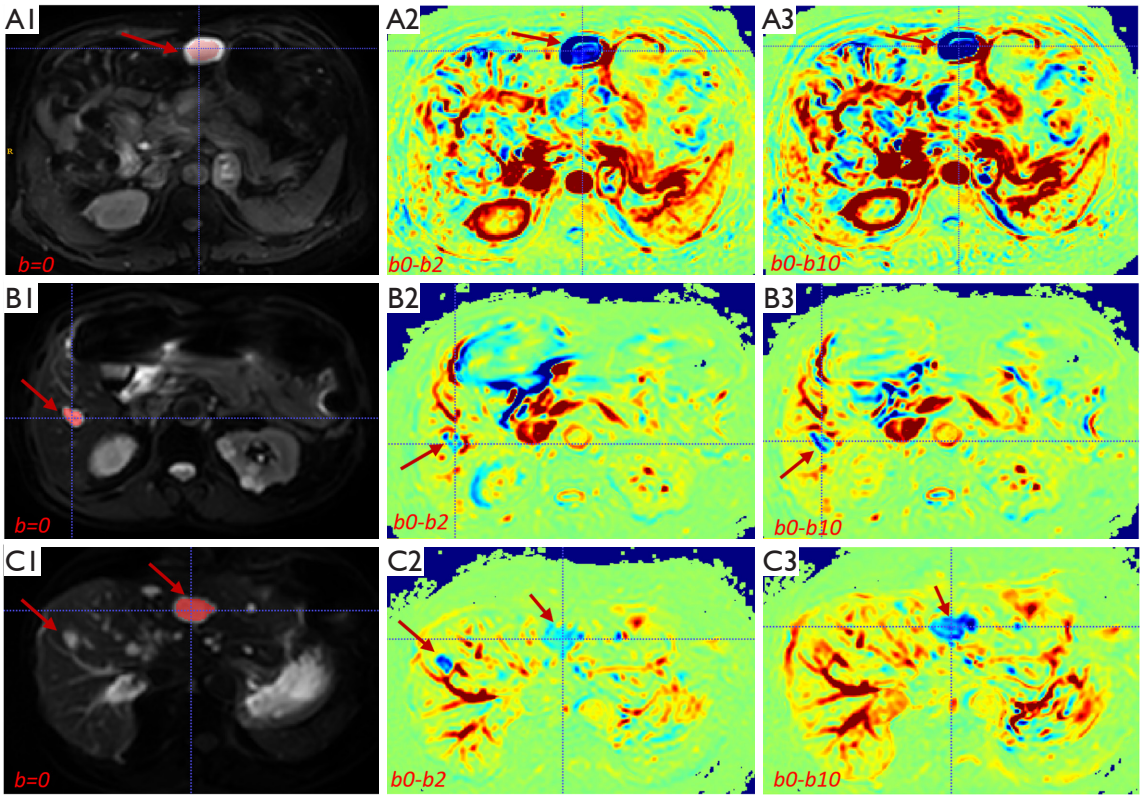

Figure 7 DDVD appearance of liver cysts (arrow) at 3.0T (four liver cysts). *b*=0 diffusion weighted image (A1,B1,C1) and DDVD pixelwise maps with the second *b*-value being 2 (A2,B2,C2) or 10 (A3,B3,C3) s/mm^2, respectively. Liver cysts typically show low DDVD signal. Three cysts were marked with region-of-interest of red color on *b*=0 diffusion weighted image. DDVD, diffusion derived 'vessel density'.

show 'no perfusion' (*Figures 4*,7). However, such a 'no perfusion' was only observed when a very low second *b*-value was applied. When the second *b*-value is higher, for example, >30 s/mm^2, liver cysts may lose their DDVD characteristics due to the contribution of T2. Note that liver cysts are likely to have a very long T2 being similar to that of gallbladder of 160 ms (53). When the second *b*-value is high, for example, 30 s/mm^2, liver cyst may show even higher DDVD signal relative to the liver parenchyma (*Figure 8*). In addition, as noted earlier (14), the '*position shift*' between the *b*=0 image and the second *b*-value image is a source of quantification error for DDVD calculation of structures inside the liver, as the liver is heavily subject to respiratory motion. One possible way to overcome this difficulty is to scan the DDVD protocol twice (or three) times, and manually select the pair of images with the most similar positions to reconstruct DDVD map. Breath-hold method DDVD data acquisition protocol may be indeed practically feasible (1).

There are many limitations to this study. This study used historical IVIM imaging data, and the 1.5T IVIM imaging data did not acquire sufficient data points between *b*=2 s/m^2 image and *b*=15 s/m^2; while the 3.0T IVIM imaging data did not acquire *b*=1 s/m^2 image. However, we expect the overall trend for the relationship between the second *b*-values and DDVDs of the liver and spleen would not be affected. Liver cyst data quantitative data were measured only with two cysts with 6 slices at 1.5T. We plan to investigate the observed phenomenon with a larger sample size, more pathological entities, and more second *b*-values.

In conclusion, this study shows the following points: (I) when the second *b*-value is very low for DDVD calculation, T2 contribution can be minimized; (II) absolute DDVD values measures higher at 3.0T than at 1.5T and the absolute DDVD difference between liver and spleen is greater at 3.0T than at 1.5T, while the ratios of $DDVD_{spleen}$ to $DDVD_{liver}$ do not apparently differ between 1.5T and 3.0T; (III) characteristic liver cyst DDVD signal is only shown with a very low second *b*-value, and when the second *b*-value is high, for example, >30 s/mm^2, liver cysts may show higher DDVD signal relative to liver parenchyma due

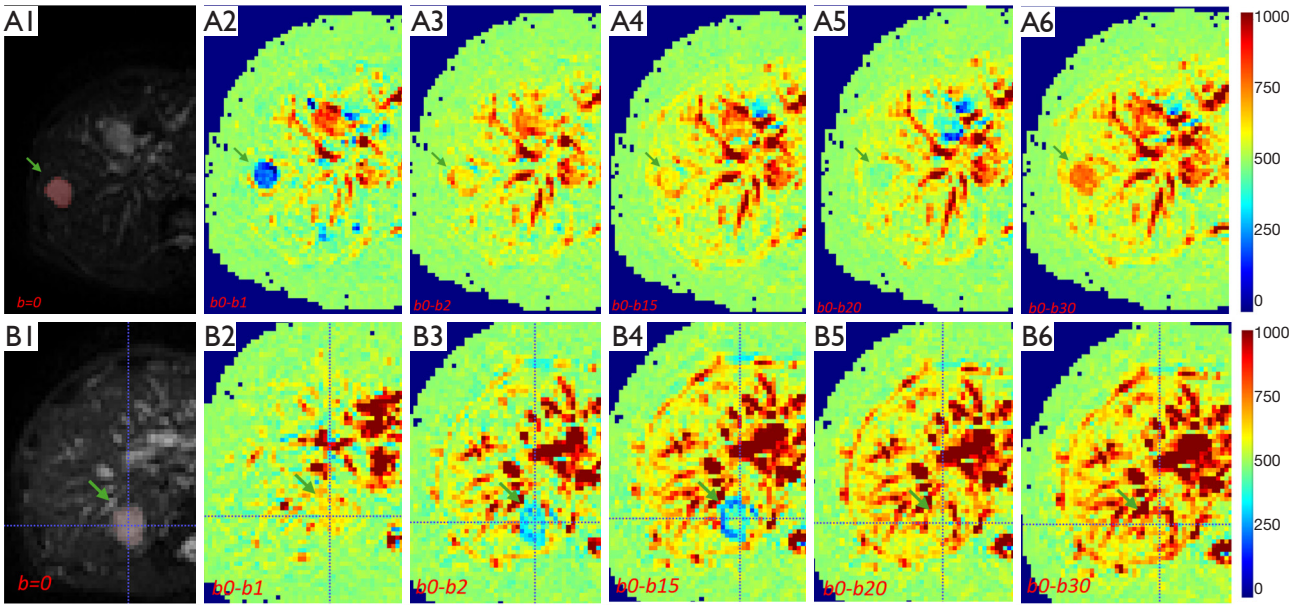

Figure 8 DDVD appearance of liver cysts (arrow) at 1.5T. *b*=0 diffusion weighted imaging (A1,B1) and DDVD pixelwise maps with the second *b*-value being 1 (A2,B2), 2 (A3,B3), 15 (A4,B4), 20 (A5,B5), and 30 s/mm^2 (A6,B6), respectively. Together due to the misalignment between *b*=0 image and the second *b*-value image and/or the T2 contribution to DDVD values, typical DDVD appearance is lost on A3, A4, A6, B2, B5, B6. DDVD, diffusion derived 'vessel density'.

to the T2 contribution.

Acknowledgments

Funding: This work was supported by a Hong Kong General Research Fund project (No. 14112521) and Shenzhen People's Hospital Physician Scientist Training "Five Three" Program (No. SYWGSLCYJ202404).

Footnote

Conflicts of Interest: All authors have completed the ICMJE uniform disclosure form (available at https://qims.amegroups.com/article/view/10.21037/qims-24-2411/coif). Y.X.J.W. serves as the Editor-in-Chief of *Quantitative Imaging in Medicine and Surgery*. G.G. serves as an unpaid editorial board member of *Quantitative Imaging in Medicine and Surgery*.Y.X.J.W. is the founder of Yingran Medicals Ltd., which develops medical image-based diagnostics software. B.H.X. and M.S.Y.Z. contributed to the development of Yingran Medicals Ltd. The other authors have no conflicts of interest to declare.

Ethical Statement: The authors are accountable for all aspects of the work in ensuring that questions related to the accuracy or integrity of any part of the work are appropriately investigated and resolved. This study reused historical image data for new analysis. All the diffusion weighed image data were acquired with the institutional ethical approval and with informed consent obtained from individual patients.

References

1. Wáng YXJ. Living tissue intravoxel incoherent motion (IVIM) diffusion MR analysis without b=0 image: an example for liver fibrosis evaluation. Quant Imaging Med Surg 2019;9:127-33.

2. Yao DQ, Zheng CJ, Deng YY, Lu BL, Lu T, Hu GW, Li XM, Xiao BH, Ma FZ, Sabarudin A, King AD, Wáng YXJ. Potential diverse applications of diffusion-derived vessel density (DDVD) pixel-by-pixel mapping. Quant Imaging Med Surg 2024;14:2136-45.
3. Huang H, Zheng CJ, Wang LF, Che-Nordin N, Wáng YXJ. Age and gender dependence of liver diffusion parameters and the possibility that intravoxel incoherent motion modeling of the perfusion component is constrained by the diffusion component. NMR Biomed 2021;34:e4449.
4. Xiao BH, Huang H, Wang LF, Qiu SW, Guo SW, Wáng YXJ. Diffusion MRI Derived per Area Vessel Density as a Surrogate Biomarker for Detecting Viral Hepatitis B-Induced Liver Fibrosis: A Proof-of-Concept Study. SLAS Technol 2020;25:474-83.
5. Hu GW, Zheng CJ, Zhong WX, Zhuang DP, Xiao BH, Wáng YXJ. Usefulness of diffusion derived vessel density computed from a simplified IVIM imaging protocol: An experimental study with rat biliary duct blockage induced liver fibrosis. Magn Reson Imaging 2021;84:115-23.
6. Zheng CJ, Huang H, Xiao BH, Li T, Wang W, Wáng YXJ. Spleen in viral Hepatitis-B liver fibrosis patients may have a reduced level of per unit micro-circulation: non-invasive diffusion MRI evidence with a surrogate marker. SLAS Technol 2022;27:187-94.
7. Gitlin N, Grahame GR, Kreel L, Williams HS, Sherlock S. Splenic blood flow and resistance in patients with cirrhosis before and after portacaval anastomoses. Gastroenterology 1970;59:208-13.
8. Oguro A, Taniguchi H, Koyama H, Tanaka H, Miyata K, Takeuchi K, Inaba T, Nakahashi H, Takahashi T. Relationship between liver function and splenic blood flow (quantitative measurement of splenic blood flow with H2(15)O and a dynamic state method: 2). Ann Nucl Med 1993;7:251-5.
9. Tsushima Y, Koizumi J, Yokoyama H, Takeda A, Kusano S. Evaluation of portal pressure by splenic perfusion measurement using dynamic CT. AJR Am J Roentgenol 1998;170:153-5.
10. Miles KA, McPherson SJ, Hayball MP. Transient splenic inhomogeneity with contrast-enhanced CT: mechanism and effect of liver disease. Radiology 1995;194:91-5.
11. He J, Chen C, Xu L, Xiao B, Chen Z, Wen T, Wáng YXJ, Liu P. Diffusion-Derived Vessel Density Computed From a Simplified Intravoxel Incoherent Motion Imaging Protocol in Pregnancies Complicated by Early Preeclampsia: A Novel Biomarker of Placental Dysfunction. Hypertension 2023;80:1658-67.
12. Li CY, Chen L, Ma FZ, Chen JQ, Zhan YF, Wáng YXJ. High performance of the diffusion MRI biomarker DDVD (diffusion-derived 'vessel density') for separating placenta associated with pre-eclampsia from placenta in normal pregnancy. Quant Imaging Med Surg 2024. doi: 10.21037/qims-24-2412.
13. Lu T, Wang L, Li M, Wang Y, Chen M, Xiao BH, Wáng YXJ. Diffusion-derived vessel density (DDVD) computed from a simple diffusion MRI protocol as a biomarker of placental blood circulation in patients with placenta accreta spectrum disorders: A proof-of-concept study. Magn Reson Imaging 2024;109:180-6.
14. Hu GW, Li CY, Zhang G, Zheng CJ, Ma FZ, Quan XY, Chen W, Sabarudin A, Zhu MSY, Li XM, Wáng YXJ. Diagnosis of liver hemangioma using magnetic resonance diffusion-derived vessel density (DDVD) pixelwise map: a preliminary descriptive study. Quant Imaging Med Surg 2024;14:8064-82.
15. Chen JQ, Li CY, Wang W, Yao DQ, Jiang RF, Wáng YXJ. Diffusion-derived vessel density (DDVD) for penumbra delineation in brain acute ischemic stroke: initial proof-of-concept results using single NEX DWI. Quant Imaging Med Surg 2024;14:9533-42.
16. Li XM, Yao DQ, Quan XY, Li M, Chen W, Wáng YXJ. Perfusion of hepatocellular carcinomas measured by diffusion-derived vessel density biomarker: Higher hepatocellular carcinoma perfusion than earlier intravoxel incoherent motion reports. NMR Biomed 2024;37:e5125.
17. Sahani DV, Holalkere NS, Mueller PR, Zhu AX. Advanced hepatocellular carcinoma: CT perfusion of liver and tumor tissue--initial experience. Radiology 2007;243:736-43.
18. Abdullah SS, Pialat JB, Wiart M, Duboeuf F, Mabrut JY, Bancel B, Rode A, Ducerf C, Baulieux J, Berthezene Y. Characterization of hepatocellular carcinoma and colorectal liver metastasis by means of perfusion MRI. J Magn Reson Imaging 2008;28:390-5.
19. Ippolito D, Capraro C, Casiraghi A, Cestari C, Sironi S. Quantitative assessment of tumour associated neovascularisation in patients with liver cirrhosis and hepatocellular carcinoma: role of dynamic-CT perfusion imaging. Eur Radiol 2012;22:803-11.
20. Lu BL, Yao DQ, Wáng YXJ, Zhang ZW, Wen ZQ, Xiao BH, Yu SP. Higher perfusion of rectum carcinoma relative to tumor-free rectal wall: quantification by a new imaging biomarker diffusion-derived vessel density (DDVD). Quant Imaging Med Surg 2024;14:3264-74.
21. Xu Y, Sun H, Song A, Yang Q, Lu X, Wang W. Predictive Significance of Tumor Grade Using 256-Slice CT Whole-Tumor Perfusion Imaging in Colorectal Adenocarcinoma.

Acad Radiol 2015;22:1529-35.
22. Sorokin EP, Basty N, Whitcher B, Liu Y, Bell JD, Cohen RL, Cule M, Thomas EL. Analysis of MRI-derived spleen iron in the UK Biobank identifies genetic variation linked to iron homeostasis and hemolysis. Am J Hum Genet 2022;109:1092-104.
23. Schwenzer NF, Machann J, Haap MM, Martirosian P, Schraml C, Liebig G, Stefan N, Häring HU, Claussen CD, Fritsche A, Schick F. T2* relaxometry in liver, pancreas, and spleen in a healthy cohort of one hundred twenty-nine subjects-correlation with age, gender, and serum ferritin. Invest Radiol 2008;43:854-60.
24. de Bazelaire CM, Duhamel GD, Rofsky NM, Alsop DC. MR imaging relaxation times of abdominal and pelvic tissues measured in vivo at 3.0 T: preliminary results. Radiology 2004;230:652-9.
25. Bogaert J, Claessen G, Dresselaers T, Masci PG, Belge C, Delcroix M, Symons R. Magnetic resonance relaxometry of the liver - a new imaging biomarker to assess right heart failure in pulmonary hypertension. J Heart Lung Transplant 2022;41:86-94.
26. Tsushima Y, Unno Y, Koizumi J, Kusano S. Measurement of human hepatic and splenic perfusion using dynamic computed tomography: a preliminary report. Comput Methods Programs Biomed 1998;57:143-6.
27. Taniguchi H, Yamaguchi A, Kunishima S, Koh T, Masuyama M, Koyama H, Oguro A, Yamagishi H. Using the spleen for time-delay correction of the input function in measuring hepatic blood flow with oxygen-15 water by dynamic PET. Ann Nucl Med 1999;13:215-21.
28. Blomley MJ, Kormano M, Coulden R, Lim-Dunham J, Dawson P, Lipton MJ. Splenic blood flow: evaluation with computed tomography. Acad Radiol 1997;4:13-20.
29. Blomley MJ, Coulden R, Dawson P, Kormano M, Donlan P, Bufkin C, Lipton MJ. Liver perfusion studied with ultrafast CT. J Comput Assist Tomogr 1995;19:424-33.
30. Bader TR, Grabenwöger F, Prokesch RW, Krause W. Measurement of hepatic perfusion with dynamic computed tomography: assessment of normal values and comparison of two methods to compensate for motion artifacts. Invest Radiol 2000;35:539-47.
31. Bader TR, Herneth AM, Blaicher W, Steininger R, Mühlbacher F, Lechner G, Grabenwöger F. Hepatic perfusion after liver transplantation: noninvasive measurement with dynamic single-section CT. Radiology 1998;209:129-34.
32. Oguro A, Taniguchi H, Koyama H, Tanaka H, Miyata K, Takeuchi K, Inaba T, Nakahashi H, Takahashi T. Relationship between liver function and splenic blood flow (quantitative measurement of splenic blood flow with H2(15)O and a dynamic state method: 2). Ann Nucl Med 1993;7:251-5.
33. Yasuhara Y, Miyauchi S, Hamamoto K. A measurement of regional portal blood flow with Xe-133 and balloon catheter in man. Eur J Nucl Med 1989;15:346-50.
34. Yu WL, Ma FZ, Huang H, Xiao BH, Li XM, Wáng YXJ. Age and gender differences of normative values of spleen diffusion MRI parameters. Rofo 2024. [Epub ahead of print]. doi: 10.1055/a-2357-9741.
35. Zhu B, Wang C, Gao J, Liu H, Li N, Teng Y. CT perfusion imaging of the liver and the spleen can identify severe portal hypertension. Abdom Radiol (NY) 2024;49:1084-91.
36. Wang L, Zhang Y, Wu YF, Yue ZD, Fan ZH, Zhang CY, Liu FQ, Dong J. Computed tomography perfusion in liver and spleen for hepatitis B virus-related portal hypertension: A correlation study with hepatic venous pressure gradient. World J Gastroenterol 2022;28:6068-77.
37. Gadupudi V, Ramachandran R, Pulivadula Mohanarangam VS. The Role of Computed Tomography Perfusion in Various Focal Liver Lesions. Cureus 2022;14:e32420.
38. Yan C, Xia C, Cao Q, Zhang J, Gao M, Han J, Liang X, Zhang M, Wang L, Zhao L. Predicting High-Risk Esophageal Varices in Cirrhosis: A Multi-Parameter Splenic CT Study. Acad Radiol 2024;31:4866-74.
39. Sauter AW, Feldmann S, Spira D, Schulze M, Klotz E, Vogel W, Claussen CD, Horger MS. Assessment of splenic perfusion in patients with malignant hematologic diseases and spleen involvement, liver cirrhosis and controls using volume perfusion CT (VPCT): a pilot study. Acad Radiol 2012;19:579-87.
40. Martirosian P, Boss A, Deimling M, Kiefer B, Schraml C, Schwenzer NF, Claussen CD, Schick F. Systematic variation of off-resonance prepulses for clinical magnetization transfer contrast imaging at 0.2, 1.5, and 3.0 tesla. Invest Radiol 2008;43:16-26.
41. Wáng YXJ, Zhao KX, Ma FZ, Xiao BH. The contribution of T2 relaxation time to MRI-derived apparent diffusion coefficient (ADC) quantification and its potential clinical implications. Quant Imaging Med Surg 2023;13:7410-6.
42. Wáng YXJ, Ma FZ. A tri-phasic relationship between T2 relaxation time and magnetic resonance imaging (MRI)-derived apparent diffusion coefficient (ADC). Quant Imaging Med Surg 2023;13:8873-80.
43. Ma FZ, Wáng YXJ. T2 relaxation time elongation of hepatocellular carcinoma relative to native liver tissue leads

to an underestimation of perfusion fraction measured by standard intravoxel incoherent motion magnetic resonance imaging. Quant Imaging Med Surg 2024;14:1316-22.
44. Wáng YXJ. Natural course of apparent diffusion coefficient (ADC) change after brain ischemic stroke: an alternative explanation by the triphasic relationship between T2 and ADC. Quant Imaging Med Surg 2024;14:9848-55.
45. Yu WL, Xiao BH, Ma FZ, Zheng CJ, Tang SN, Wáng YXJ. Underestimation of the spleen perfusion fraction by intravoxel incoherent motion MRI. NMR Biomed 2023;36:e4987.
46. Wáng YXJ, Aparisi Gómez MP, Ruiz Santiago F, Bazzocchi A. The relevance of T2 relaxation time in interpreting MRI apparent diffusion coefficient (ADC) map for musculoskeletal structures. Quant Imaging Med Surg 2023;13:7657-66.
47. Huang H, Che-Nordin N, Wang LF, Xiao BH, Chevallier O, Yun YX, Guo SW, Wáng YXJ. High performance of intravoxel incoherent motion diffusion MRI in detecting viral hepatitis-b induced liver fibrosis. Ann Transl Med 2019;7:39.
48. FZ Ma, BH Xiao, Wang YXJ. Signal simulation of liver DDVD (diffusion derived 'vessel density') with multiple compartments diffusion MRI model. Quant Imaging Med Surg 2024. doi: 10.21037/qims-24-2693.
49. Kim BR, Song JS, Choi EJ, Hwang SB, Hwang HP. Diffusion-Weighted Imaging of Upper Abdominal Organs Acquired with Multiple B-Value Combinations: Value of Normalization Using Spleen as the Reference Organ. Korean J Radiol 2018;19:389-96.
50. Ohtomo K, Itai Y, Furui S, Yashiro N, Yoshikawa K, Iio M. Hepatic tumors: differentiation by transverse relaxation time (T2) of magnetic resonance imaging. Radiology 1985;155:421-3.
51. Reimer P, Weissleder R, Brady TJ, Yeager AE, Baldwin BH, Tennant BC, Wittenberg J. Experimental hepatocellular carcinoma: MR receptor imaging. Radiology 1991;180:641-5.
52. Onaya H, Itai Y, Ahmadi T, Yoshioka H, Okumura T, Akine Y, Tsuji H, Tsujii H. Recurrent hepatocellular carcinoma versus radiation-induced hepatic injury: differential diagnosis with MR imaging. Magn Reson Imaging 2001;19:41-6.
53. Cieszanowski A, Szeszkowski W, Golebiowski M, Bielecki DK, Grodzicki M, Pruszynski B. Discrimination of benign from malignant hepatic lesions based on their T2-relaxation times calculated from moderately T2-weighted turbo SE sequence. Eur Radiol 2002;12:2273-9.

Cite this article as: Ju ZG, Leng XM, Xiao BH, Sun MH, Huang H, Hu GW, Zhang G, Sun JH, Zhu MSY, Guglielmi G, Wáng YXJ. Influences of the second motion probing gradient b-value and T2 relaxation time on magnetic resonance diffusion-derived 'vessel density' (DDVD) calculation: the examples of liver, spleen, and liver simple cyst. Quant Imaging Med Surg 2025;15(1):74-87. doi: 10.21037/qims-24-2411

